Graphene-embedded waveguide with improved modulation capability

PENG Xi-Liang[1*], YANG Xin[2]

（1. Department of Research and development, Nanjing Research Institute of Electronic Technology,
Nanjing 210039, China;
2. School of Medicine, Southeast University, Nanjing 210009, China）

Abstract：A graphene-embedded waveguide (GEW) with improved modulation capability was proposed, which can be over 2 times larger than that of conventional graphene-on-silicon (GOS) waveguide. More importantly, it is found that the improvement of modulation capability mainly results from the enhanced electric field confinement around graphene. Based on this finding, we propose a high-efficient method to optimize the modulation capability. By using this method, the optimization work can be reduced by an order of magnitude. Our work may promote the design of graphene-based electro-optic modulator with high modulation capability.

Key words：graphene, modulator, optimization, waveguide

PACS: 78. 67. Wj, 42. 79. Hp

调制能力提升的嵌入式石墨烯波导结构

彭希亮[1*]，仰　欣[2]
（1. 南京电子技术研究所 研究部，江苏 南京 210039；
2. 东南大学 医学院，江苏 南京 210009）

摘要：提出了一种调制能力提升的嵌入式石墨烯波导结构(GEW)。相对于传统的石墨烯覆盖硅表面波导结构(GOS)，其调制能力可以提升 2 倍以上。更重要的是发现电场在 GEW 中可以被更好地束缚在石墨烯上，这正是 GEW 的调制能力获得显著提升的主要原因。基于上述发现，进一步提出了一种高效的调制能力优化方法。通过采用该方法，优化工作的计算量可以减少 1 个数量级。综上所述，本文的工作可能对将来研究者设计拥有高调制能力的石墨烯电光调制器提供一定帮助。

关　键　词：石墨烯；调制器；优化；波导

中图分类号：TN256　　　**文献标识码**：A

Introduction

In current integrated optoelectronic circuits, electro-optic modulator is an essential component performing electro-optic conversion. For the modulator based on electro-absorption (EA) effect, the modulation is realized by tuning the absorption of the waveguide. Hence, the performance of EA modulator depends on the change of propagation loss per unit length, i. e. the amplitude modulation capability (AMC). For the modulator based on electro-refraction (ER) effect, the modulation is realized by tuning the propagation phase to control the resonance [1-5] or the interference [6-7] of the light. Therefore, the performance of ER modulator depends on the change of propagation phase per unit length, i. e. the phase modulation capability (PMC). Nevertheless, the AMC and PMC of traditional silicon waveguide are quite small due to the weak EA effect and ER effect in silicon. Hence, a quite long silicon waveguide is required, e. g. a typical silicon modulator usually needs the length of ~1 mm [8]. Furthermore, it is not cost-efficient to integrate such a large silicon modulator in a chip.

In order to reduce the footprint of electro-optic modulator, the GOS waveguide modulator has been proposed due to its enhanced AMC (~ 0. 07 dB/μm) and PMC (~ 1. 1 deg/μm) [9]. However, it is found that the interaction between propagating light and graphene is relatively

weak in the GOS waveguide modulator [10-15]. This is because most of the electric field is confined in the silicon waveguide and has little interaction with the top graphene layer [16-19]. Therefore, the AMC and PMC can be improved further only if the electric field can be confined around graphene by using an elaborately designed waveguide modulator structure.

In this work, a GEW with improved AMC and PMC is proposed. The AMC and PMC of GEW can be 3 and 2 times larger than those of traditional GOS waveguide respectively. The improvement is achieved by enhancing the electric field confinement around graphene. As a result, the footprint of the modulator based on GEW can be more compact than that based on GOS. Moreover, a high-efficient method to optimize the AMC and PMC of GEW is proposed. Based on this method, the optimization work can be cut down by an order of magnitude.

1 Structure

The structure of GEW is shown in Fig. 1 (a). A silicon layer with a width of W_{GEW} and a height of H_{GEW} is on the silica substrate. Monolayer graphene is embedded into a 14-nm-thickness aluminum oxide layer which is in the center of silicon. Besides, graphene is modeled as anisotropic material shown as the Appendix. Its out-of-plane relative permittivity $\varepsilon_{\perp}$ is fixed at 2.5 while its in-plane relative permittivity $\varepsilon_{//}$ varies with chemical potential μ_c which can be tuned by external voltage [20] (the detail can be found in the Appendix). By using the eigen mode analysis at optical communication wavelength 1550 nm, the transverse electric (TE) mode of GEW is shown in Fig. 1 (b) (in-plane electric field intensity $E_{//} = \left(\left| E_x \right|^2 + \left| E_y \right|^2 \right)^{1/2}$) and Fig. 1 (c) (out-of-plane electric field intensity $E_{\perp} = \left| E_z \right|$).
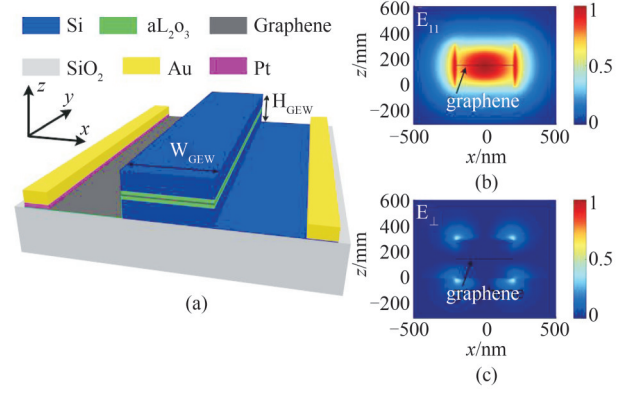

Fig. 1 (a) The schematic diagram of the GEW, (b) in-plane electric field distribution for TE mode, and (c) out-of-plane electric field distribution for TE mode
图1 (a) GEM的示意图,(b) TE模式的面内电场分布,(c) TE模式的面外电场分布

2 Principle

When the TE mode propagates along GEW, its loss per micron γ and phase change per micron ϕ can be expressed as

$$\gamma(dB/\mu m) = 40\pi \lg(e) \operatorname{Im}(n_{eff})/(10^6 \lambda), \quad (1)$$

and

$$\phi(deg/\mu m) = 360 \operatorname{Re}(n_{eff})/(10^6 \lambda) \quad , \quad (2)$$

respectively, where λ is the wavelength, n_{eff} is the effective mode index of TE mode. Furthermore, the AMC and PMC of GEW can be expressed as

$$AMC = \Delta\gamma = 40\pi \lg(e) \operatorname{Im}(\Delta n_{eff})/(10^6 \lambda), \quad (3)$$

and

$$PMC = \Delta\phi = 360 \operatorname{Re}(\Delta n_{eff})/(10^6 \lambda) \quad , \quad (4)$$

where Δn_{eff} is the change of effective mode index induced by the variation of μ_c. According to electromagnetic theory [21-22], n_{eff} can be approximated as

$$n_{eff} = \sqrt{\frac{D_{eff}}{E_{eff}}} = \sqrt{\frac{\oiint \varepsilon_{Si} E_{Si} dS_{Si} + \oiint \varepsilon_{Al_2O_3} E_{Al_2O_3} dS_{Al_2O_3} + \oiint \varepsilon_{SiO_2} E_{SiO_2} dS_{SiO_2} + \oiint \varepsilon_{air} E_{air} dS_{air} + \oiint \varepsilon_g E_g dS_g}{\oiint E_{Si} dS_{Si} + \oiint E_{Al_2O_3} dS_{Al_2O_3} + \oiint E_{SiO_2} dS_{SiO_2} + \oiint E_{air} dS_{air} + \oiint E_g dS_g}} \quad . \quad (5)$$

In Eq. 5, ε_{Si}, $\varepsilon_{Al_2O_3}$, ε_{SiO_2}, ε_{air} and ε_g are the relative permittivity of Si, Al_2O_3, SiO_2, air and graphene respectively. E_{Si}, $E_{Al_2O_3}$, E_{SiO_2}, E_{air} and E_g are the electric field intensity inside the region of Si, Al_2O_3, SiO_2, air and graphene respectively. S_{Si}, $S_{Al_2O_3}$, S_{SiO_2}, S_{air} and S_g are the area for the region of Si, Al_2O_3, SiO_2, air and graphene respectively. Because the $E_{\perp}$ on graphene is much smaller than the $E_{//}$ on graphene shown as Fig 1. (b) and Fig 1. (c). Therefore, the $E_{\perp}$ on graphene can be ignored, which means $\oiint \varepsilon_g E_g dS_g$ and $\oiint E_g dS_g$ can be approximated as $\oiint \varepsilon_{//} E_{//} dS_g$ and $\oiint E_{//} dS_g$ respectively. Hence, n_{eff} can be further expressed as

$$n_{eff} = \sqrt{\frac{D_p + \varepsilon_{//} I_g}{I_t}} \quad , \quad (6)$$

where $D_p = \oiint \varepsilon_{Si} E_{Si} dS_{Si} + \oiint \varepsilon_{Al_2O_3} E_{Al_2O_3} dS_{Al_2O_3} + \oiint \varepsilon_{SiO_2} E_{SiO_2} dS_{SiO_2} + \oiint \varepsilon_{air} E_{air} dS_{air}$, $I_g = \oiint E_{//} dS_g$ and $I_t = \oiint E_{Si} dS_{Si} + \oiint E_{Al_2O_3} dS_{Al_2O_3} + \oiint E_{SiO_2} dS_{SiO_2} + \oiint E_{air} dS_{air} + \oiint E_{//} dS_g$. Because

the electric field integration in graphene is much smaller than the sum of electric field integration in the whole waveguide, I_g/I_t will approach 0. Based on the Taylor's series expansion, the n_{eff} can be approximated as

$$n_{eff} \approx \sqrt{D_p/I_t} \left[1 + \varepsilon_{//} I_g/(2D_p) \right] \quad . \quad (7)$$

Because of the ultrathin thickness of graphene, it is assumed that the variation of graphene permittivity nearly does not change the field distribution. Therefore, Δn_{eff} can be expressed as

$$\Delta n_{eff} = \sqrt{D_p/I_t} I_g \Delta\varepsilon_{//}/(2D_p) \quad . \quad (8)$$

By substituting Eq. 8 into Eq. 3 and Eq. 4, the AMC and PMC can be expressed as

$$AMC = \frac{20\pi \lg(e) \sqrt{D_p/I_t}}{(10^6 \lambda)} \operatorname{Im}\left(\frac{I_g \varepsilon_0 \Delta\varepsilon_{//}}{\varepsilon_0 D_p} \right), \quad (9)$$

and

$$\mathrm{PMC} = \frac{180\sqrt{D_p/I_t}}{10^6\lambda} \mathrm{Re}\left(\frac{I_g \varepsilon_0 \Delta\varepsilon_{/\!/}}{\varepsilon_0 D_p}\right) \quad, \quad (10)$$

respectively. Since most of the electric field is in the silicon region, $\sqrt{D_p/I_t}$ is estimated to be near the refractive index of silicon. According to Eqs. 9-10, it is found that the modulation capability (MC) including AMC and PMC mainly depends on the normalized changeable electric displacement field $I_g \varepsilon_0 \Delta\varepsilon_{/\!/}/(\varepsilon_0 D_p)$, i. e. the ratio of the changed electric displacement field caused by graphene to the electric displacement field in the whole waveguide except graphene. Hence, the AMC and PMC can be improved by enlarging the factor $\kappa = I_g/D_p$, which means the electric field needs to be confined in graphene region as much as possible.

3 Optimization

In order to optimize the AMC and PMC of GEW, a sweep of the geometrical parameters including the waveguide height H_{GEW} and the chemical potential of graphene μ_c under different waveguide width W_{GEW} is taken. In the following discussion, graphene is set to be at the center of silicon while sweeping H_{GEW} ranging from 100 nm to 800 nm with an increase step of 20 nm and μ_c ranging from 0 eV to 1 eV with an increase step of 0. 05 eV. The n_{eff} and field distribution are obtained from numerical simulation. Then the AMC, PMC and κ can be calculated with Eqs. 3-4 and the equation $\kappa = I_g/D_p$, respectively.

In traditional method, locally maximum AMC and PMC at each H_{GEW} need to be found by sweeping μ_c[16-18]. By comparing these locally optimized AMC and PMC under different H_{GEW}, the globally optimized AMC and PMC can be found. Therefore, the total sets of simulation will be $M \times N$=756, where M=36 is the number of H_{GEW} and N =21 is the number of μ_c. However, this optimization strategy usually requires long simulation time and huge storage space.

In order to relieve the simulation burden, a high-efficient optimization method based on the physical understanding of MC is proposed. On the one hand, AMC and PMC mainly depend on $\Delta\varepsilon_{/\!/}$ and κ as Eqs. 9-10 show. On the other hand, $\Delta\varepsilon_{/\!/}$ is mainly determined by μ_c and κ is mainly determined by electric field distribution varying with geometric parameters. Hence, the AMC and PMC can be optimized by sweeping μ_c and H_{GEW} independently. First, M simulations are set under different H_{GEW} (shown as the blue square in Fig. 2 (a-f) or Fig. 3 (a-f)) to find the H^*_{GEW} where κ reaches its maximum. After fixing H_{GEW} at H^*_{GEW}, N simulations are set under different μ_c to find the best AMC and PMC. Hence, the total sets of simulation are only $M + N$=57. Comparing to traditional optimization method ($M \times N$=756), the simulation time and memory requirement can be cut down by at least 1 order of magnitude.

In Figs. 2 (a-f), the AMC first increases with H_{GEW} then decreases with H_{GEW}. Meanwhile, the peak of AMC gradually moves to the point of smaller H_{GEW} as W_{GEW} in-
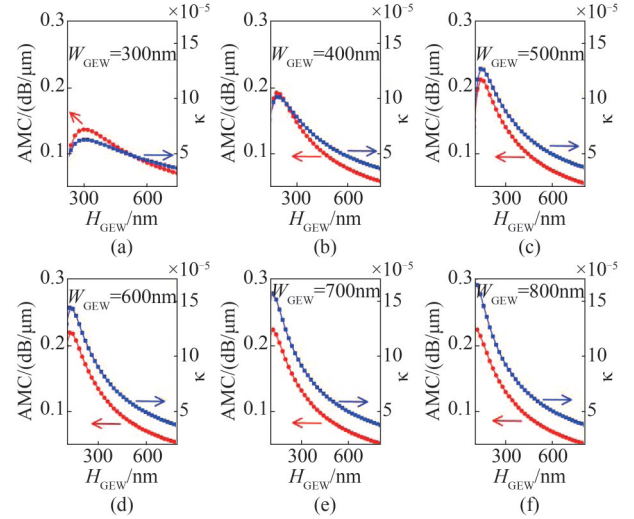

Fig. 2   The AMC (red circle) and κ (blue square) varies with the H_{GEW} at (a) W_{GEW} =300 nm, (b) W_{GEW} =400 nm; (c) W_{GEW} =500 nm, (d) W_{GEW} =600 nm, (e) W_{GEW} =700 nm, (f) W_{GEW} =800 nm
图2   AMC(红色圆圈)和κ(蓝色正方形)随着HGEW改变而变化 (a) W_{GEW} =300 nm,(b) W_{GEW} =400 nm,(c) W_{GEW} =500 nm,(d) W_{GEW} =600 nm,(e) W_{GEW} =700 nm,(f) W_{GEW} =800 nm
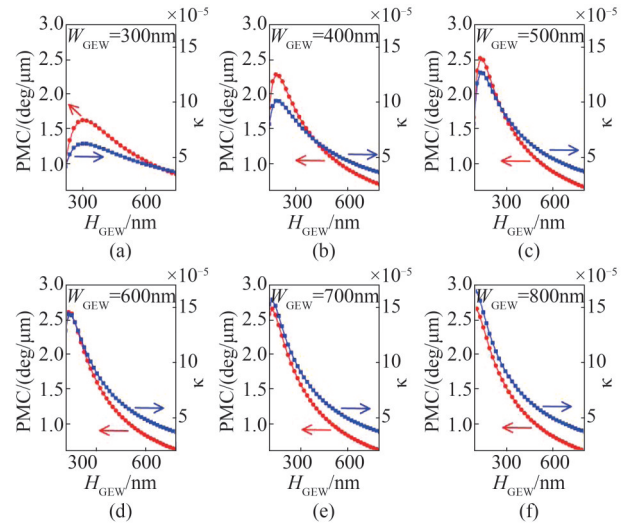

Fig. 3   The PMC (red circle) and κ (blue square) varies with the H_{GEW} at (a) W_{GEW}=300 nm, (b) W_{GEW} =400 nm, (c) W_{GEW} = 500 nm, (d) W_{GEW} =600 nm, (e) W_{GEW} =700 nm, (f) W_{GEW} =800 nm
图3   PMC(红色圆圈)和κ(蓝色正方形)随着HGEW的改变而变化 (a) W_{GEW} =300 nm,(b) W_{GEW} =400 nm,(c) W_{GEW} =500 nm,(d)W_{GEW}=600 nm,(e)W_{GEW}=700 nm,(f)W_{GEW}=800 nm

creases. It is also found that the locally optimized AMC increases with W_{GEW} but the increment will be smaller and smaller. At W_{GEW}=800 nm and H_{GEW}=100 nm, the globally optimized AMC is found to be ~0. 224 dB/μm, which is over 3 times larger than the AMC of a typical GOS waveguide[9]. As a result, the length of the EA modulator based on the optimized GEW can be reduced over 67% accordingly.

Similar high-efficient optimization method can also be used to optimize the PMC as Figs. 3 (a-f) shows. It is

found that the best PMC=~2. 66 deg/μm is also reached at W_{GEW}=800 nm and H_{GEW}=100 nm. The PMC of the optimized GEW is over 2 times larger than the PMC of the GOS waveguide [9]. In Fig. 4 (a), a Mach-Zehnder interferometer (MZI) modulator based on the optimized GEW (W_{GEW}=800 nm, H_{GEW}=100 nm) is proposed. Its optical transmission is given as:

$$\text{Tr} = \left(e^{-2\pi L \text{Im}\left(n_{eff}^{A}\right)/\lambda} + e^{-2\pi L \text{Im}\left(n_{eff}^{B}\right)/\lambda} \right)/4 +$$

$$0.5 e^{-\pi \text{Im}\left(n_{eff}^{A} + n_{eff}^{B}\right)L/\lambda} \cos\left[2\pi L \text{Re}\left(n_{eff}^{A} - n_{eff}^{B}\right)/\lambda \right], \quad (11)$$

where L=100 μm is length of interferometer arms, n_{eff}^{A} and n_{eff}^{B} are the n_{eff} of the two arms[9]. By fixing the applied voltage on the arm A as ~6. 1 V and tuning the applied voltage on the arm B from ~6. 1 V to ~1. 9 V, the phase difference between two arms varies from $0°$ to $180°$. Accordingly, the transmission of the MZI decreases from 94. 8% (binary state "1") to 1. 3% (binary state "0") shown as Fig. 4 (b). However, the applied voltage to realize $180°$ phase difference for the MZI based on GOS waveguide will be as large as ~32. 0 V [9]. Hence, the MZI based on the optimized GEW can be more energy-efficient.
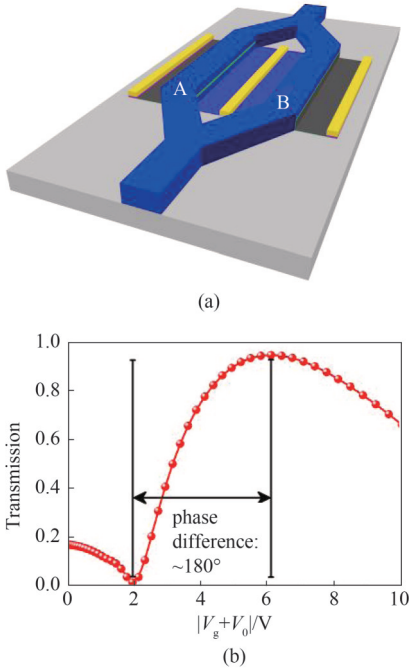

(a)

(b)

Fig. 4 (a) The schematic diagram of MZI based on optimized GEW (W_{GEW}=800 nm, H_{GEW} =100 nm), (b) Transmission of MZI based on the optimized GEW as a function of the applied voltage $\left| V_g + V_0 \right|$

图 4 (a)基于优化后 GEM 的 MZI 调制器原理图(W_{GEW}=800 nm, W_{GEW} =100 nm),(b) 基于优化后 GEM 的 MZI 调制器,其传输率将随着石墨烯上的电压| V_g+V_0 |的变化而改变

In order to improve the modulation efficiency further, the structure which can provide larger κ should be used. As reported in previous study [17], the κ can be enlarged significantly by using the plasmonic waveguide and the self-biased graphene stacks. Since larger κ

means more electric field is confined in graphene, the AMC of a typical graphene modulator based on plasmonic waveguide can be increased to as large as 0. 84 dB/μm [17]. However, a large optical loss of 0. 09 dB/μm should be taken care of and a special coupler needs to be added, which may lead to a more complicated design [17].

4 Conclusion

In summary, the physical understanding for the modulation capability (including AMC and PMC) of GEW is provided in this paper. The normalized changeable electric displacement field is found to be the main determining factor for the modulation capability. Based on this finding, a high-efficient method to optimize the modulation capability is proposed. By using the proposed optimization method instead of traditional method, the simulation time and storage space can be cut down by at least 1 order of magnitude. After optimization, the AMC or PMC of GEW can be over 3 or 2 times larger than those of a typical GOS waveguide respectively. Hence, a more compact or energy-efficient modulator can be achieved. This work may pave the way for designing graphene-based electro-optic modulator with large modulation capability.

5 Appendix

Here, graphene is modeled as an anisotropic material. Its out-of-plane relative permittivity $\varepsilon_{\perp}$ is 2. 5 and in-plane relative permittivity $\varepsilon_{\parallel}$ is

$$\varepsilon_{\parallel} = 1 + \frac{i\sigma_g}{\omega d_g \varepsilon_0} \quad , \quad (12)$$

where σ_g is the surface conductivity of graphene, ω is the angular frequency, d_g=0. 34 nm is the thickness of graphene and ε_0 is the permittivity in free space [23]. Based on Kubo formula, σ_g can be calculated as

$$\sigma_g = \frac{-ie^2}{\pi\hbar^2(\omega + i2\Gamma)} \int_0^{\infty} \varepsilon \left(\frac{\partial f_d(\varepsilon)}{\partial \varepsilon} - \frac{\partial f_d(-\varepsilon)}{\partial \varepsilon} \right) d\varepsilon +$$

$$\frac{-ie^2(\omega + i2\Gamma)}{\pi\hbar^2} \int_0^{\infty} \frac{f_d(\varepsilon) - f_d(-\varepsilon)}{(\omega + i2\Gamma)^2 - 4\left(\frac{\varepsilon}{\hbar} \right)^2} d\varepsilon \quad , \quad (13)$$

where e is the charge of electron, $\hbar$ is the reduced Planck's constant, Γ is the scattering rate and $f_d(\varepsilon)$ is the Fermi-Dirac function [24]. Furthermore, $f_d(\varepsilon)$ can be expressed as

$$f_d(\varepsilon) = \frac{1}{\exp\left[\left(\varepsilon - \mu_c \right)/\left(k_B T \right) \right] + 1} \quad , \quad (14)$$

where μ_c is the chemical potential of graphene, k_B is the Boltzmann constant and T=300 K is the temperature [23]. Moreover, μ_c can be controlled by the external voltage:

$$\mu_c = \hbar v_F \sqrt{\eta\pi \left| V_g + V_0 \right|} \quad , \quad (15)$$

where $\eta = 9 \times 10^{16} \text{m}^{-2}\text{V}^{-1}$ is estimated with a parallel-plate capacitor model, $v_F = 0. 9 \times 10^6 \text{ms}^{-1}$ is the Fermi velocity, V_g is the driven voltage and V_0 is the voltage offset due to natural doping [25]. For simplicity but not losing

principle，$\left|V_g + V_0\right|$ can be considered as the applied voltage on graphene.

According to Eqs. 12-15，it is found that the $\varepsilon_{/\!/}$ can be modified by varying μ_c，which can be further tuned by changing the applied voltage shown as Fig. 5.
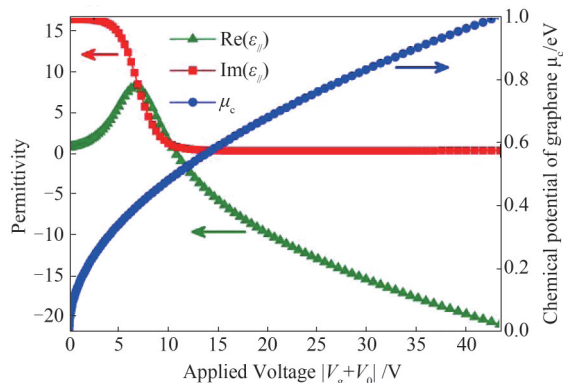

Fig. 5   The real part of $\varepsilon_{/\!/}$ （green triangle），the imaginary part of $\varepsilon_{/\!/}$ （red square）and the chemical potential of graphene μ_c （blue circle）

图5 $\varepsilon_{/\!/}$ 的实部(绿色三角形)，$\varepsilon_{/\!/}$ 的虚部(红色正方形)以及石墨烯的化学式μ_c(蓝色圆圈)

References

［1］Zhou F，Wen H. Performance analysis and optimization of TM/TE independent graphene ring modulator ［J］. *Optical and Quantum Electronics*，2021，**53**(8)：1-10.

［2］Shekhawat D，Mehra R. Design of ultra-compact and highly-sensitive graphene assisted silicon micro-ring resonator modulator for switching applications ［J］. *Silicon*，2021：1-8.

［3］Xue H，Guo S，Li Z，*et al*. Tunable Fano resonance based on graphene U-shaped double-microring resonator ［J］. *Optical Engineering*，2020，**59**(12)：127104.

［4］Zhou F，Liang C. Highly tunable and broadband graphene ring modulator ［J］. *Journal of Nanophotonics*，2019，**13**(1)：016008.

［5］Ghods M M，Afsahi M. Design and simulation of the optical amplitude-shift keying modulator using Fabry – Perot resonator coupled with graphene at near-infrared frequencies ［J］. *Journal of Nanophotonics*，2021，**15**(2)：026006.

［6］CHEN R G，LIN R，SHEN L M，*et al*. 3-μm mid-infrared polarization-independent and CMOS-compatible graphene modulator ［J］. *Journal of Infrared and Millimeter Waves*(陈荣国，林瑞，沈黎明，等。3-μm中红外偏振无关且CMOS兼容的石墨烯调制器，**红外与毫米波学报**)，2021，**40**(3)：297.

［7］Armaghani S，Khani S，Danaie M. Design of all-optical graphene switches based on a Mach-Zehnder interferometer employing optical Kerr effect ［J］. *Superlattices and Microstructures*，2019，**135**：106244.

［8］Thomson D J，Gardes F Y，Fedeli J-M，*et al*. 50-Gb/s silicon optical modulator ［J］. *IEEE Photonics Technology Letters*，2011，**24**(4)：234-6.

［9］Phatak A，Cheng Z，Qin C，*et al*. Design of electro-optic modulators based on graphene-on-silicon slot waveguides ［J］. *Optics letters*，2016，**41**(11)：2501-4.

［10］Hao R，Jiao J，Peng X，*et al*. Experimental demonstration of a graphene-based hybrid plasmonic modulator ［J］. *Optics letters*，2019，**44**(10)：2586-9.

［11］Liu J，Khan Z U，Wang C，*et al*. Review of graphene modulators from the low to the high figure of merits ［J］. *Journal of Physics D*：*Applied Physics*，2020，**53**(23)：233002.

［12］Liu J，Khan Z U，Sarjoghian S. Metal-clad-suspended self-biasing graphene modulator with tunable figure of merit ［J］. *Journal of Optics*，2020，**49**(3)：364-9.

［13］Karimkhani H，Vahed H. Hybrid broadband optical modulator based on multi-layer graphene structure and silver nano-ribbons ［J］. *Optical and Quantum Electronics*，2020，**52**(5)：1-11.

［14］Cheng Z，Zhu X，Galili M，*et al*. Double-layer graphene on photonic crystal waveguide electro-absorption modulator with 12 GHz bandwidth ［J］. *Nanophotonics*，2020，**9**(8)：2377-85.

［15］Najafi-hajivar M，Hosseini-Farzad M. Broadband polarization-insensitive amplitude and phase modulators based on graphene-covered buried and ridge silicon waveguides ［J］. *Optics Communications*，2020，**472**：125860.

［16］Jiao J，Hao R，Zhen Z，*et al*. Optimization of graphene-based slot waveguides for efficient modulation ［J］. *IEEE Journal of Selected Topics in Quantum Electronics*，2019，**26**(2)：1-5.

［17］Peng X，Hao R，Ye Z，*et al*. Highly efficient graphene-on-gap modulator by employing the hybrid plasmonic effect ［J］. *Optics Letters*，2017，**42**(9)：1736-9.

［18］Zhu Y，Deng C，Huang L，*et al*. Hybrid plasmonic graphene modulator with buried silicon waveguide ［J］. *Optics Communications*，2020，**456**：124559.

［19］Chakraborty I，Roy S，Dixit V，*et al*. Atto-joule energy-efficient graphene modulator using asymmetric plasmonic slot waveguide ［J］. *Photonics and Nanostructures-Fundamentals and Applications*，2021，**43**：100865.

［20］Li Z，Huang J，Zhao Z，*et al*. Single-layer graphene optical modulator based on arrayed hybrid plasmonic nanowires ［J］. *Optics Express*，2021，**29**(19)：30104-13.

［21］Hao R，Du W，Chen H，*et al*. Ultra-compact optical modulator by graphene induced electro-refraction effect ［J］. *Applied Physics Letters*，2013，**103**(6)：061116.

［22］Zhou F，Hao R，Jin X-F，*et al*. A graphene-enhanced fiber-optic phase modulator with large linear dynamic range ［J］. *IEEE Photonics Technology Letters*，2014，**26**(18)：1867-70.

［23］Rezaei M H，Shiri M. High-performance tunable resonant electro-optical modulator based on suspended graphene waveguides ［J］. *Optics Express*，2021，**29**(11)：16299-311.

［24］Wang J，Qiu H，Wei Z，*et al*. Design of a graphene-based waveguide-integrated multimode phase modulator ［J］. *IEEE Photonics Journal*，2021，**13**(4)：1-6.

［25］Wang J，Zhang X，Chen Y，*et al*. Design of a graphene-based silicon nitride multimode waveguide-integrated electro-optic modulator ［J］. *Optics Communications*，2021，**481**：126531.